Enhancement of Multiplexing Capability of Low-Coherence Interferometric Fiber Sensor Array by Use of a Loop Topology

Libo Yuan, Wei Jin, *Senior Member, IEEE*, Limin Zhou, Y. L. Hoo, and M. S. Demokan, *Senior Member, IEEE*

***Abstract*—A novel technique for enhancing the multiplexing capability of low-coherence interferometric sensor array is proposed. The technique uses a fiber loop topology and allows for twice as many sensors as the conventional low-coherence reflectometry system to be multiplexed. Power budget and signal analyses for different sizes of sensor array are performed. A ten-sensor system was experimentally demonstrated and applied for quasi-distributed temperature measurement. An additional advantage of the technique is that it provides an extra degree of redundancy through the bidirectional interrogation of the sensor array and thus improves the system reliability.**

***Index Terms*—Fiber-optic interferometer, loop topology, low-coherence reflectometry, multiplexing techniques, optical fiber sensors, redundancy, strain/temperature measurements.**

I. Intruduction

OPTICAL low-coherence reflectometry (OLCR) or optical coherence domain reflectometry (OCDR) is based on a Michelson interferometer with a broad-band source, i.e., a source with a short coherence length. The OLCR concept was first introduced in 1987 [1], [2] as a high-resolution measurement technique to probe optical devices for optical communication applications. The OLCR has been applied to measure the reflection properties of optical waveguides [3], fibers [4], [5], and biological structures [6]. The use of low coherence interferometry for sensor applications can be traced back to an even earlier date [7]. The attraction of low-coherence interferometry for sensing applications is its ability to multiplex in the coherence domain many sensor signals onto a single fiber-optic data bus without requiring the use of relatively complex time- or frequency-division-multiplexing techniques [8]–[10]. The coherence-multiplexing schemes [11]–[14] typically use separate receiving interferometers whose optical path differences (OPDs) are matched to that of the remote sensing interferometers.

The objective of this paper is to demonstrate a technique that is capable of enhancing the multiplexing capability [11] of the low-coherence interferometric sensor array through the use of a fiberloop topology. The use of loop topology allows bidirectional interrogation of each of the sensors in the array from opposite directions and thus ensures the normal operation of the system, even when one of the sensors in the array is damaged.

Manuscript received May 3, 2002; revised January 29, 2003. This work was supported by the Teaching and Research Award Program for Outstanding Young Professors in Higher Education Institute, MOE, China; the Science Foundation of Heilongjiang Province for Outstanding Youth, 1999; the National Natural Science Foundation of China under Grant 50179007 to the Harbin Engineering University; and the Hong Kong Polytechnic University under Grants G-W099 and G-YC64.

L. Yuan is with the Department of Physics, Harbin Engineering University, Harbin 150001, China, and also with the Department of Mechanical Engineering, The Hong Kong Polytechnic University, Hong Kong, China (e-mail: lbyuan@vip.sina.com).

W. Jin, Y. L. Hoo, and M. S. Demokan are with the Department of Electrical Engineering, The Hong Kong Polytechnic University, Hong Kong, China.

L. Zhou is with the Department of Mechanical Engineering, The Hong Kong Polytechnic University, Hong Kong, China.

Digital Object Identifier 10.1109/JLT.2003.810918

II. Description of the Multiplexing Technique

A. System Configuration

Fig. 1 shows a schematic of the proposed multiplexing setup. Light from a broad-band amplified spontaneous emission (ASE) source is launched, via a fiber-optic isolator, into a fiber loop through the use of a 3-dB loop coupler. N segments of sensing fibers $(S_1, S_2, \ldots, S_N)$ are connected in serial and further connected to the arms of the loop coupler to form the sensing loop. Light returned from the sensing loop is coupled into a scanning receiving interferometer within an OLCR. The receiving interferometer is of Michelson type and is formed by using a 3-dB coupler with one arm (the lower arm) connected to a reference fiber with a mirrored end and the other arm (the upper arm) to a pigtailed fiber collimator followed by a scanning mirror. Light signals reflected from both mirrors are combined at the 3-dB coupler and detected by a photodetector (PD).

B. Basic Principle

For each sensing segment (e.g., segment S_{i} or sensor S_{i}, as shown in Fig. 1), there are four reflected waves associated with it, two returning from the clockwise (CW) direction and two from the counterclockwise (CCW) direction. The two CW (or CCW) reflected waves correspond to reflections occurring at the two ends of the sensing sensors that are connected to the adjacent segments. The OPD between the two CW reflected waves is the same as that between the CCW waves and equals to twice the optical path of the sensing segment. If the OPD of the receiving interferometer is made equal or matched, by the use of the scanning mirror, to the OPD of the reflected waves as mentioned previously, a white light interference fringe will be produced. The mirror position that corresponds to the peak of the fringe pattern can then be used as a measure of the OPD of the sensing segment.

0733-8724/03$17.00 © 2003 IEEE

Authorized licensed use limited to: IEEE Xplore. Downloaded on October 22, 2008 at 22:21 from IEEE Xplore. Restrictions apply.

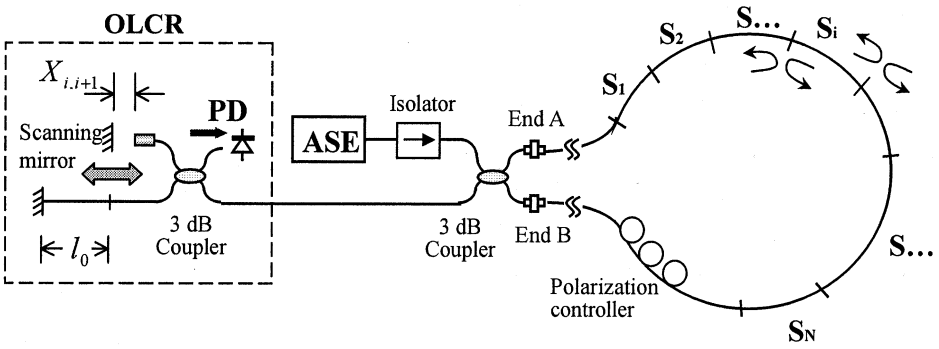

Fig. 1. Schematic of the proposed multiplexing setup.

For the N-sensor loop shown in Fig. 1, there would be N interference fringes when the OPD of the receiving interferometer is scanned. The positions of the scanning mirror at the peaks of the N fringes correspond to the optical path matches of the receiving interferometer to that of the sensors and can then be used to recover the OPD of the N sensing segments. The lengths of the sensing segments can be chosen arbitrarily as long as the difference between the longest and shortest is within the scanning range of the OLCR. To avoid crosstalk between signals from different sensors, the length of each segment should be chosen differently. The reflectivities at the joints between the adjacent segments should be made small to avoid depletion of the probe signal. A detailed analysis on optical paths, peak fringe intensities, and applications for strain and temperature measurements will be presented in the next section.

III. Signal Analysis

A. Optical Path Analysis

Fig. 2 shows the optical paths and the reflected waves associated with sensor $S_{\rm i}$. The 3-dB loop coupler splits input light into two, one travels along CW and the other in a CCW direction toward the sensing segment $S_{\rm i}$. The CW light travels through the coupler arm L_A and passes through a series of sensing segments $(S_1, S_2, \ldots, S_{i-1})$ before reaching segment $S_{\rm i}$. This light signal is reflected at the two ends of the segment $S_{\rm i}$, and the two reflected waves return through the same path to the loop coupler and then go into the receiving interferometer. Similarly, the CCW light travels through the coupler arm L_B and a serial of segments $(S_N, S_{N-1}, \ldots, S_{i+1})$ and is reflected at the ends of the segment $S_{\rm i}$. The return light goes into the same receiving interferometer. The interference fringe corresponding to $S_{\rm i}$ is due to a path match of the two groups (CW and CCW) of the aforementioned reflected waves. For the CW light, the paths that are matched are

$$2nL_A+2n\sum_{k=0}^{i} l_{k,k+1}+nL_{\rm com}+2nL_E+2nl_0 \quad (1)$$

$$2nL_A+2n\sum_{k=0}^{i} l_{k,k+1}+nL_{\rm com}+2nL_D+2nl_{i,i+1}+2X_{i,i+1} \quad (2)$$

where n is the refractive index of the fiber, L_A and L_B are the coupler arm lengths that connects the first and the last sensing segments, $l_{i,i+1}$ is the gauge length of $S_{\rm i}$, and $X_{i,i+1}$ is the gap distance between the fiber collimator and the scanning mirror. The definitions of other parameters used in (1) and (2) are labeled in Fig. 2. For the CCW light, the matched two paths are

$$2nL_B+2n\sum_{k=i+1}^{N} l_{k,k+1}+nL_{\rm com}+2nL_E+2nl_0 \quad (3)$$

and

$$2nL_B+2n\sum_{k=i+1}^{N} l_{k,k+1}+nL_{\rm com} +2nL_D+2nl_{i,i+1}+2X_{i,i+1}. \quad (4)$$

The value of $X_{i,i+1}$ that corresponds the path match of $S_{\rm i}$ can be obtained by setting the optical paths given in (1) and (3) to be equal to that of (2) and (4), respectively, and expressed as

$$X_{i,i+1} = n(L_D - L_E) + n(l_{i,i+1} - l_0) \quad (5)$$

where L_D and L_E are constant lengths and can be made approximately equal. The variation in the OPD of $S_{\rm i}$ can then be measured by tracing the change of the mirror displacement $\Delta X_{i,i+1}$, i.e.,

$$\Delta X_{i,i+1} = \Delta(nl_{i,i+1}). \quad (6)$$

B. Intensity of Interference Fringe

Assume that light intensity from the source, just after the isolator, is I_0. The light intensity return to the PD after traveling through the optical path given in (1) may be expressed as

$$I_{\rm CW}(i)=\frac{I_0}{16}\left\{\prod_{k=0}^{i-1} T_k\beta_k\right\}R_i\left\{\prod_{k=0}^{i-1} T_k'\beta'\right\}R_f, \quad i=0,1,2,\ldots,N. \quad (7)$$

The light intensity at the PD through the optical path given in (2) is given by

$$I_{\rm CW}(i+1) = \frac{I_0}{16}\left\{\prod_{k=0}^{i-1} T_k\beta_k\right\} R_i \left\{\prod_{k=0}^{i-1} T_k'\beta'\right\} \eta(X_{i,i+1})R_m, \quad i=0,1,2,\ldots,Nr \quad (8)$$

where the excess insertion losses of the couplers are neglected. β_i represents the excess loss associated with segment $S_{\rm i}$, including the connection loss between the sensing segments. T_i

Authorized licensed use limited to: IEEE Xplore. Downloaded on October 22, 2008 at 22:21 from IEEE Xplore. Restrictions apply.

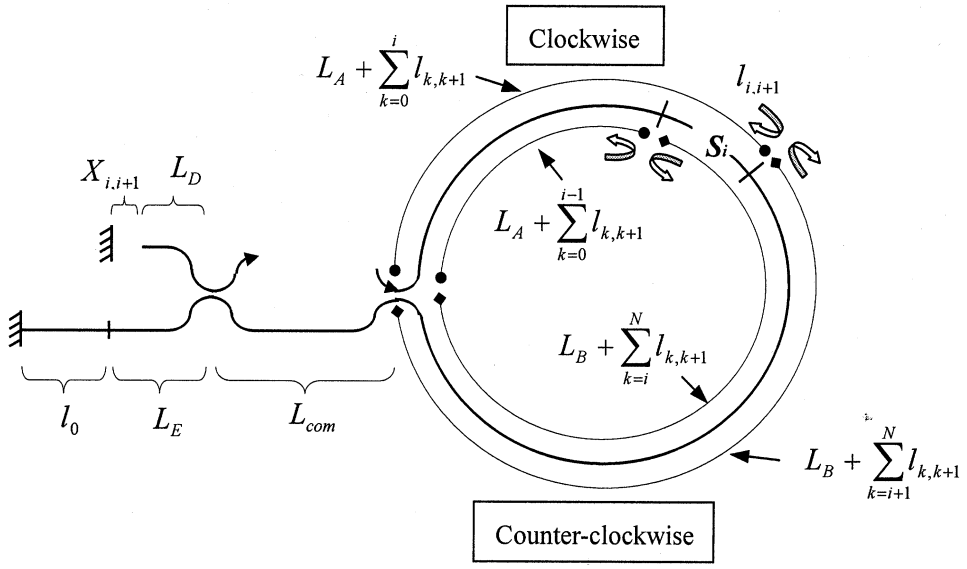

Fig. 2. Illustration of the optical paths associated with sensing segment S_i.

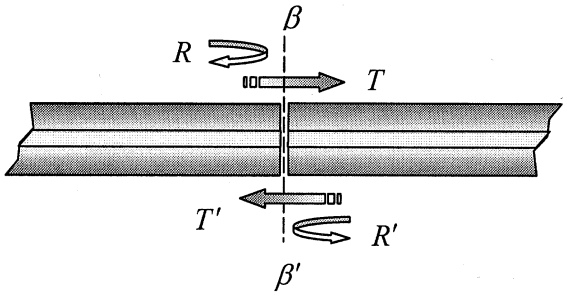

Fig. 3. Reflection, transmission, and excess insertion loss occur at a fiber joint.

and R_i are the transmission and reflection coefficients of the joint between S_{i-1} and S_i, respectively. T_i is, in general, smaller than $1 - R_i$ because of the loss factor β_i. $\eta(X_{i,i+1})$ is the loss associated with the scanning mirror and fiber-optic collimator system and is a function of $X_{i,i+1}$. R_f and R_m are the reflectivities of the mirrored reference fiber end and scanning mirror, respectively. β_i', T_i', and R_i' represent the loss, the transmission, and the reflection coefficients from the CCW direction , respectively, as shown in Fig. 3.

To simplify the expression, we assume that

$$\begin{cases} R_i = R_i' \\ T_i = T_i' \\ \beta_i = \beta_i'. \end{cases} \tag{9}$$

Equations (7) and (8) can then be simplified as

$$I_{\mathrm{CW}}(i) = \frac{I_0}{16}\left\{\prod_{k=0}^{i-1} T_k\beta_k\right\}^2 R_i R_f, \quad i = 0,1,2,\ldots,N \tag{10}$$

$$I_{\mathrm{CW}}(i+1) = \frac{I_0}{16}\left\{\prod_{k=0}^{i} T_k\beta_k\right\}^2 R_{i+1}\eta(X_{i,i+1})R_m, \quad i = 0,1,2,\ldots,N. \tag{11}$$

Similarly, light intensity at the PD after traveling through the two CCW paths, as given in (3) and (4), can be written as

$$I_{\mathrm{CCW}}(i) = \frac{I_0}{16}\left\{\prod_{k=i}^{N+1} T_k\beta_k\right\}^2 R_i R_f, \quad i = 0,1,2,\ldots,N \tag{12}$$

$$I_{\mathrm{CCW}}(i+1) = \frac{I_0}{16}\left\{\prod_{k=i+1}^{N+1} T_k\beta_k\right\}^2 R_{i+1}\eta(X_{i,i+1})R_m, \quad i = 0,1,2,\ldots,N. \tag{13}$$

The light signal that is used to perform measurement is the coherent mixing terms of the reflected light signals from the sensors' matching paths; the peak fringe intensity may be expressed as

$$\begin{aligned} I_D(i) &= 2\sqrt{I_{\mathrm{CW}}(i)I_{\mathrm{CW}}(i+1)} + 2\sqrt{I_{\mathrm{CCW}}(i)I_{\mathrm{CCW}}(i+1)} \\ &= \frac{I_0}{8}\sqrt{R_f R_m R_i R_{i+1}\eta(X_{i,i+1})} \\ &\quad \times\left\{T_i\beta_i\left[\prod_{k=0}^{i} T_k\beta_k\right]^2 + T_{i+1}\beta_{i+1}\left[\prod_{k=i+1}^{N+1} T_k\beta_k\right]^2\right\}. \end{aligned} \tag{14}$$

C. Applications for Strain and Temperature Sensing

1) Quasi-Distributed Strain Measurement: Assume a distributed strain field is applied to the sensor array and the sensor gauge length $l_{i,i+1}$ $(i = 0,1,2,\ldots,N)$ is changed to $l_{i,i+1} + \Delta l_{i,i+1}$. The variation in the scanning mirror position $(\Delta X_{i,i+1})$ can then be related to the strain field by

$$\Delta X_{i,i+1} = n\Delta l_{i,i+1}(\varepsilon_{i,i+1}) + l_{i,i+1}\Delta n(\varepsilon_{i,i+1}), \quad i = 0,1,2,\ldots,N. \tag{15}$$

The first term $n\Delta l_{i,i+1}(\varepsilon_{i,i+1})$ in (15) represents a change in the physical length and can be related to the applied axial strain

Authorized licensed use limited to: IEEE Xplore. Downloaded on October 22, 2008 at 22:21 from IEEE Xplore. Restrictions apply.

$\varepsilon_{i,i+1}$ through the expression $\Delta l_{i,i+1}(\varepsilon_{i,i+1}) = l_{i,i+1}\varepsilon_{i,i+1}$. The second term is the change in optical path due to a change in the refractive index of the fiber, which is given by [15]

$$\Delta n(\varepsilon_{i,i+1}) = -\frac{1}{2}n^3\left[(1-\mu)p_{12} - \mu p_{11}\right]\varepsilon_{i,i+1} \tag{16}$$

where μ is Poisson's ratio of the fiber material. p_{ij} is the elements of the strain-optic tensor of the fiber material. For silica fiber at wavelength $\lambda = 1300$ nm, the parameters n, μ, p_{11}, and p_{12} are equal to 1.46, 0.25, 0.12, and 0.27, respectively [15].

From (16) and (15), a direct relationship between the strain applied to sensor $S_{\rm i}$ and the displacement of the scanning mirror can be obtained as

$$\varepsilon_{i,i+1} = \eta(n)\frac{\Delta X_{i,i+1}}{l_{i,i+1}} \tag{17}$$

where $\eta(n) = n\{1-(1/2)n^2[(1-\mu)p_{12} - \mu p_{11}]\} \approx 1.19$ [12]. If the value of $\Delta X_{i,i+1}(i = 0,1,2,\ldots,N)$ can be measured, the strains applied to all the sensors can be recovered by using (17).

2) Quasi-Distributed Temperature Monitoring: Assume that the temperature applied to segment $S_{\rm i}$ is changed from T_0 to $T_{i,i+1}$, the optical path of the segment will vary due to the thermal expansion of the fiber and the change in refractive index of the fiber. The relationship between the scanning mirror displacement $\Delta X_{i,i+1}$ and the temperature variation $T_{i,i+1} - T_0$ may be obtained by using (6) as

$$\Delta X_{i,i+1} = n(T_0)l_{i,i+1}(T_0)[\alpha_T + C_T](T_{i,i+1} - T_0). \tag{18}$$

The temperature applied to sensor $S_{\rm i}$ can then be calculated if $\Delta X_{i,i+1}$ can be measured

$$T_{i,i+1} = \frac{\Delta X_{i,i+1}}{n(T_0)l_{i,i+1}(T_0)[\alpha_T + C_T]} + T_0, \quad i = 0,1,2,\ldots,N \tag{19}$$

where $n(T_0)$ is the refractive index of fiber at temperature T_0, and α_T and C_T are the thermal expansion coefficient and the temperature coefficient of the fiber refractive index, respectively. For the standard single-mode fiber at wavelength $\lambda = 1300$ and 1550 nm, the parameters are $n = 1.4681$ (at 25°C), $\alpha_T = 5.5 \times 10^{-7}/°\text{C}$, $C_T = 0.762 \times 10^{-5}/°\text{C}$, and $n = 1.4675$ (at 25°C), $\alpha_T = 5.5 \times 10^{-7}/°\text{C}$, $C_T = 0.811 \times 10^{-5}/°\text{C}$ [16], respectively.

IV. Multiplexing Capacity Evaluation

The peak fringe intensity or signal intensity of individual sensors within the array can be calculated using (14). Assume that the insertion loss coefficient associated with sensor $S_{\rm i}$ is $\beta_i = 0.9 (i = 0,1,2,\ldots,N)$. Under the condition of perpendicular incidence, the reflectivity at the fiber end surface is given by Fresnel formula $R = (n-1)^2/(n+1)^2$. The typical value of fiber core index is $n = 1.46$, corresponding to 4% reflectivity. For good butt-connected fiber ends, the air gap is smaller than a wavelength. In this case, R is smaller and may be approximately regarded as 1%. The transmission coefficient T_i can then be calculated as $T_i = 0.89$. Assume that the average attenuation of the scanning mirror/collimator system is 6 dB, i.e., $\eta(X_{i,i+1}) = 1/4$. We then calculated the normalized signal intensity distribution $I_D(i)/\underset{j=0,1,2,\ldots N}{\rm Max}\{I_D(j)\}(i = 0,1,2,\ldots N)$ for various sizes of sensor array. The results are shown in Fig. 4. For comparison, the normalized signal intensity distributions for both the closed- and the open-loop cases for sensor size $N = 10$ are shown in Fig. 5. The results for the open-loop cases were also obtained from (14) with one of the terms in the bracket being dropped. Obviously, the signal intensities for the closed-loop case are, in general, higher than that for the open-loop cases.

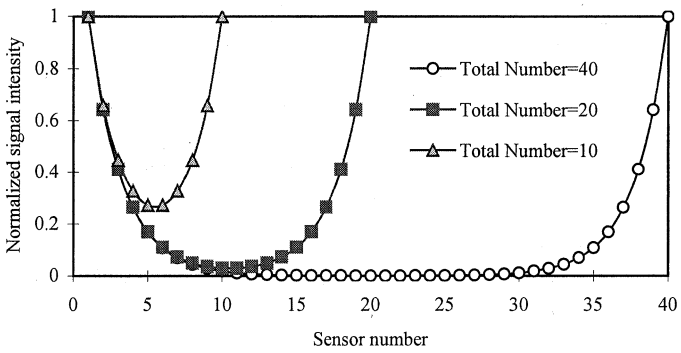

Fig. 4. Normalized signal intensity distribution within an array of 10, 20, and 40 sensors.

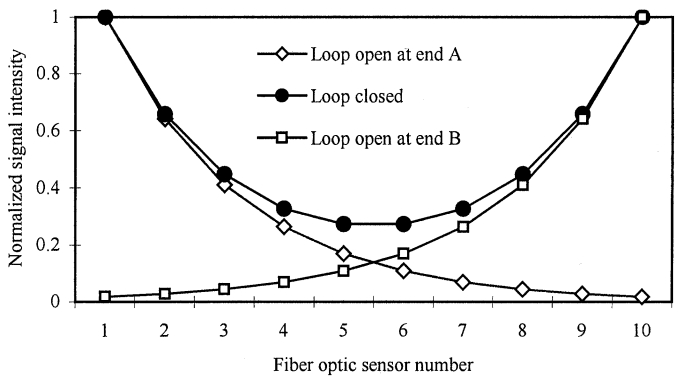

Fig. 5. Comparison of signal intensity distribution for a ten-sensor array when the loop is on a closed or an open state.

It can be seen that the signal intensity for individual sensors in the array are different. To ensure normal operation of the sensor array, the signal intensity of all the sensors within the array should be well above the noise floor of the photoreceiver. Assume that the minimum light intensity required for the system to function normally is $I_{\rm min}$; the maximum sensor number can then be evaluated by using the condition

$$I_D(i) \geq I_{\rm min}. \tag{20}$$

The typical detecting capability of the photodiode is about 1 nW. Taking into account the noise floor and other stray signals in the system, a reasonable detect limit may be $I_{\rm min} = 10$ nW. For a light source power $I_0 = 50$ μW, the maximum sensor number that satisfies condition (20) can be obtained using (14) to be $N_{\rm max} = 17$ for the closed-loop case and $N_{\rm max} = 7$ for the open-loop case. For light source power $I_0 = 3$ mW, we have $N_{\rm max} = 35$ and $N_{\rm max} = 16$, respectively, for the closed- and the open-loop cases. The relationship between maximum sensor

Authorized licensed use limited to: IEEE Xplore. Downloaded on October 22, 2008 at 22:21 from IEEE Xplore. Restrictions apply.

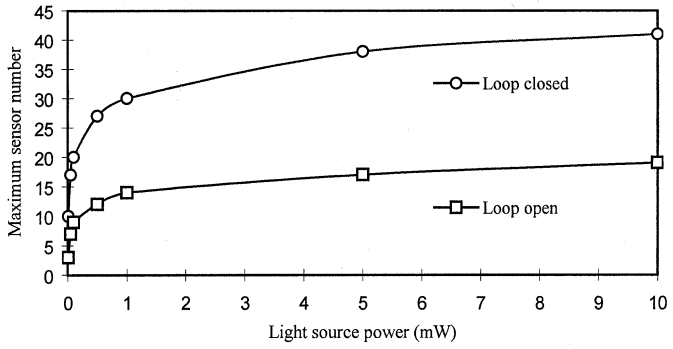

Fig. 6. Maximum sensor number versus power level of the light source.

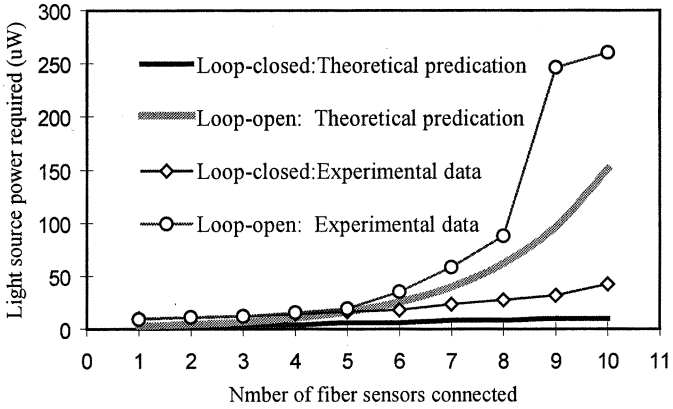

Fig. 7. Required minimum source power level versus the number of sensors connected in the loop.

number that can be multiplexed and source power is plotted in Fig. 6.

It should be mentioned that the number of sensors that can be multiplexed also depend on other factors, such as the maximum displacement range of the scanning mirror. The receiver noise floor, which depends on the receiver bandwidth and is affected by the speed of the scanning mirror, is another limiting factor. The maximum sensor number may then be less than that predicted by (20). Fig. 7 shows the calculated and measured minimum source power required as functions of the number of sensors connected in the array. The experimental measured values are considerably larger than that of the theoretical predictions. The experimental procedures used to obtain the measured data in Fig. 7 will be reported in the next section.

V. Experiments and Results

Experiments were conducted using the setup shown in Fig. 1. The power level of the erbiium-doped fiber ASE is adjustable in the range of 0 $\sim$ 10 mW. Ten fiber segments were butt-connected in serial to form the sensing array. The gauge lengths of the sensing segments are approximately 1 m with a length difference between the adjacent segments of about 7 mm. Fig. 8 shows the typical outputs of the scanning interferometer for a source power of 0.47 dBm. Fig. 8(a) and (b) corresponds to the cases when the loop was closed and open, respectively, at end A. These results agree qualitatively with the theoretical results shown in Fig. 5. The discrepancy in the signal amplitudes may

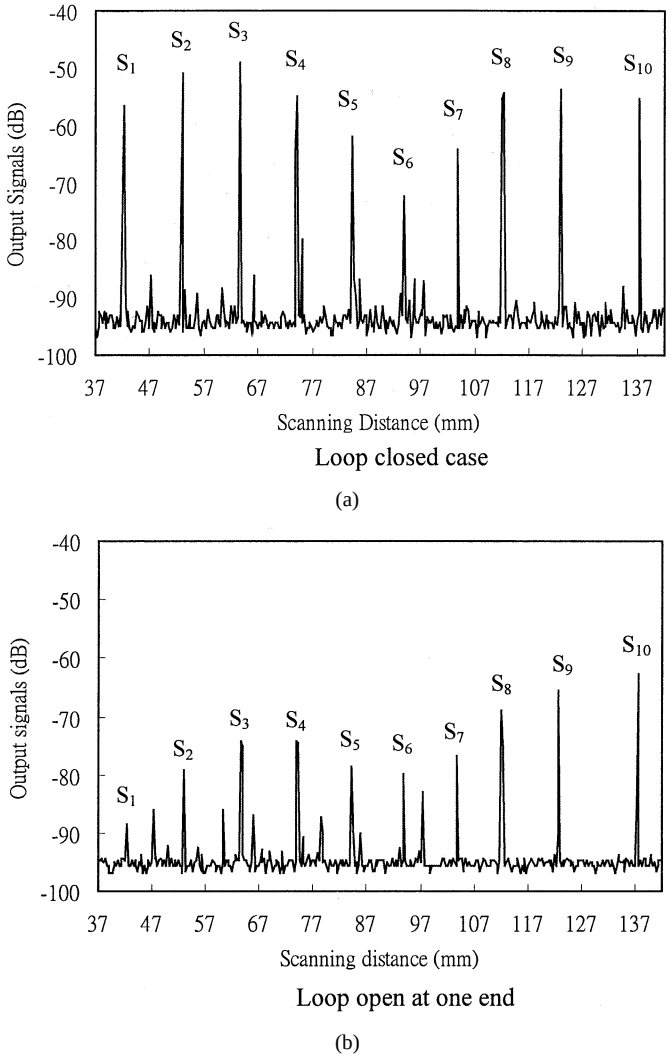

Fig. 8. Output signal from a ten-sensor array with source power level of 0.47 dBm.

be due to the fact that reflectivities at the joints between the segments, which was difficult to control exactly, are different from that used in the theoretical calculations.

It can be seen that the results shown in Fig. 8(a) and (b) essentially provide the same measurement information in terms of the positions of the peaks. This means that the system would function the same, even when one end of the loop is opened. The signal level for the closed-loop case is, however, higher than that for the open-loop case. For the particular light level of 0.47 dBm, the signal level for sensor S_1 is obviously small when the loop was open at end A [Fig. 8(b)]. Similarly, the signal level of sensor S_{10} would be small if the loop were opened at end B. The signal level was significantly enhanced for the closed-loop case [Fig. 8(a)]. Obviously, for the same source power level and receiver noise floor, the maximum sensor number can be increased with the closed-loop configuration.

The minimum required source power level as a function of the connected sensor number was investigated by connecting the sensor segments one by one from segment 1 to 10 and adjusting the light source power until the last sensor's signal can be recognized (5 dB above the noise floor). The results are shown in Fig. 7, together with the theoretical prediction from

Authorized licensed use limited to: IEEE Xplore. Downloaded on October 22, 2008 at 22:21 from IEEE Xplore. Restrictions apply.

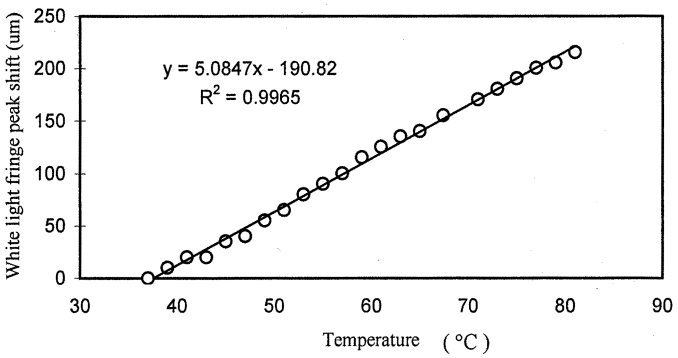

Fig. 9. Temperature calibration results for a fiber of gauge length of 500 mm.

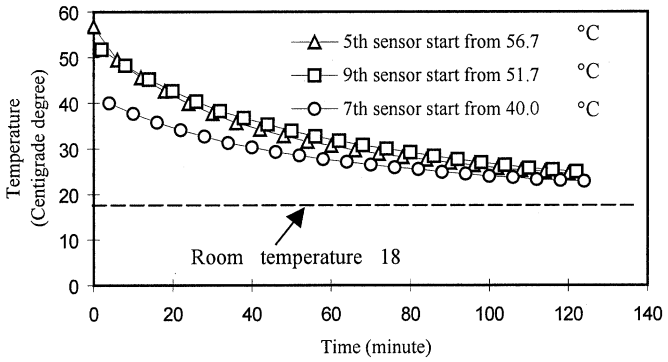

Fig. 10. Results of the temperature distribution measurement.

Section IV. The experimentally measured power level is considerably bigger than that predicated by the theoretical calculation because of the simplification made in the theoretical model.

The sensor array shown in Fig. 1 was used for quasi-distributed temperature measurements. The temperature calibration experiment was firstly carried out by emerging a 500-mm-long fiber segment into a hot water bath and measuring the shift in the fringe peak and at the same time the water temperature by using a thermal couple located near the sensing fiber. The linear relationship between the peak shift of the white-light interference fringe and the temperature given by the thermocouple over a range from 35°C to 85°C is plotted in Fig. 9. The calibration coefficient can be calculated as 10.17 (μm/m ·° C). We then put fifth, seventh, and ninth fiber-optic sensors in separate water baths with different starting temperatures and then cool them down. The remaining seven sensors were kept at room temperature (18°C). The measured results using the looped fiber sensor array are plotted in Fig. 10. It can be seen that the sensor array can map the variation in the temperature distribution. The seven sensors that were not emerged in the water baths showed no shift in the interference fringe positions.

VI. Discussion

Although the measurement results for the cases where the loop is open at either end A or end B is polarization-independent (in the strict sense, the effect of polarization is negligible), the results obtained from the closed-loop measurements are affected by the polarization states of light within the loop. Fig. 11

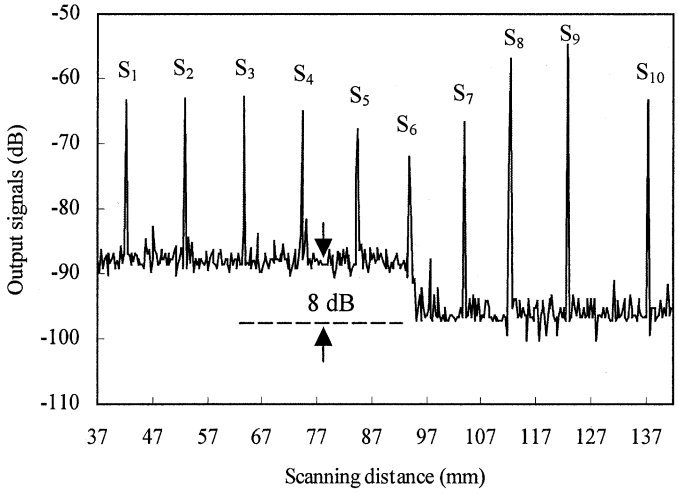

Fig. 11. Output signal of the ten-sensor array with a source power level of 0.47 dBm. An 8-dB reduction in the noise floor is achieved by adjusting the polarization state.

shows the variation of the output signals when the polarization controller within the loop (see Fig. 1) was adjusted. An 8-dB reduction in the noise floor was achieved by adjusting the polarization state of light within the loop. The variation of the noise floor with polarization state is because that light signals that are not reflected at joints between the segments would travel through the fiber loop and combine at the loop coupler. As the counterpropagating signals travel through the same fiber loop in opposite directions, the OPD between them is approximately zero. When the counterpropagating light signals are of the same polarization states, the light signal at the output port of the loop would approach zero due to destructive interference [17]. When the counterpropagating signals are of different polarization, the orthogonal polarization components would add up in intensity and result in a noise floor. As the applied strain, temperature, and other environmental disturbances would affect the state of polarization, the output polarization states of the counterpropagating waves at the loop coupler could be time varying and thus cause random fluctuation of the noise floor. The multiplexing capability would then be reduced if no countermeasures were taken to control the polarization states. This problem can be minimized or overcome by introducing a depolarizer between the ASE light source, using a sensing loop made from polarization-maintaining fiber.

VII. Conclusion

A technique for improving the multiplexing capability has been proposed. The technique is based on the bidirectional interrogation of a loop topology sensor array. A practical implementation using an OLCR and standard single-mode fiber was demonstrated. The sensing loop topology is completely passive, and absolute length measurements can be obtained for each one of the sensing segments. Although experiments were conducted using ten sensing segments of ~1-m length. Theoretical calculation shows that up to 40 sensors could be multiplexed if a broad-band source when 10-mW power is used. The gauge length of the sensing segments can be much longer, as long as a

Authorized licensed use limited to: IEEE Xplore. Downloaded on October 22, 2008 at 22:21 from IEEE Xplore. Restrictions apply.

similar length of matching fiber is used in the receiving interferometer. The sensing system can be used to measure quasi-distribution strain or temperature over large-scale structures. The use of bidirectional interrogation of the sensor array allows the normal operation of the sensing system, even when the sensing fiber is broken at a point in the loop and thus improves the system reliability.

REFERENCES

[1] R. C. Younquist, S. Catt, and D. E. N. Davies, "Optical coherence-domain reflectometry: A new optical evaluation technique," *Opt. Lett.*, vol. 12, pp. 158–160, 1987.

[2] B. L. Danielson and C. D. Whittenberg, "Guided-wave reflectometry with micrometer resolution," *Appl. Opt.*, vol. 26, p. 2836, 1987.

[3] K. Takada, I. Yokohama, K. Chida, and J. Noda, "New measurement system for fault location in optical waveguide devices based on an interferometric technique," *Appl. Opt.*, vol. 26, p. 1603, 1987.

[4] L. Thevenaz, J. P. Pellaux, and J. P. von der Weid, "All-fiber interferometer for chromatic dispersion measurements," *J. Lightwave Technol.*, vol. 6, pp. 1–7, Jan. 1988.

[5] K. Takada, K. Yukimatsu, M. Kobayashi, and J. Noda, *Appl. Phys. Lett.*, vol. 59, p. 143, 1991.

[6] X. Clivaz, F. Marquis-Weible, R. P. Salathe, R. P. Novak, and H. H. Gilgen, "High-resolution reflectometry in biological tissues," *Opt. Lett.*, vol. 17, pp. 4–6, 1992.

[7] S. A. Al-Chalabi, B. Culshaw, and D. E. N. Davies, "Partially coherent sources in interferometry," in *Proc. Inst. Elect. Eng. 1st Int. Conf. Optical Fiber Sensors*, London, U.K., 1983, pp. 132–135.

[8] J. L. Brooks, R. H. Wentworth, R. C. Youngquist, M. Tur, B. Y. Kim, and H. J. Shaw, "Coherence multiplexing of fiber optic interferometric sensors," *J. Lightwave Technol.*, vol. LT-3, pp. 1062–1071, Oct. 1985.

[9] A. B. L. Ribeiro and D. A. Jackson, "Low coherence fiber optic system for remote sensors illuminated by a 1.3 μm multimode laser diode," *Rev. Sci. Instrum.*, vol. 64, pp. 2974–2977, 1993.

[10] D. Inaudi, A. Elamari, L. Pflug, N. Gisin, J. Breguet, and S. Vurpillot, "Low-coherence deformation sensors for the monitoring of civil-engineering structures," *Sens. Actuators A, Phys.*, vol. 44, pp. 125–130, 1994.

[11] W. V. Sorin and D. M. Baney, "Multiplexing sensing using optical low-coherence reflectometry," *IEEE Photon. Technol. Lett.*, vol. 7, pp. 917–919, Aug. 1995.

[12] L. B. Yuan and F. Ansari, "White light interferometric fiber-optic distributed strain-sensing system," *Sens. Actuators A, Phys.*, vol. 63, pp. 177–181, 1997.

[13] L. B. Yuan and L. Zhou, "1 $\times$ N star coupler as distributed fiber optic strain sensor using in white light interferometer," *Appl. Opt.*, vol. 37, pp. 4168–4172, 1998.

[14] L. B. Yuan, L. Zhou, and W. Jin, "Quasidistributed strain sensing with white-light interferometry: A novel approach," *Opt. Lett.*, vol. 25, pp. 1074–1076, 2000.

[15] C. D. Butter and G. B. Hocker, "Fiber optic strain gauge," *Appl. Opt.*, vol. 17, pp. 2867–2869, 1978.

[16] L. B. Yuan, "Effect of temperature and strain on fiber optic refractive index," *Acta Optica Sinica*, vol. 17, pp. 1713–1717, 1997.

[17] W. Jin, "Fiber optic gyroscope," in *Guided Wave Optical Sensors*, W. Jin, Y. Liao, and Z. Zhang, Eds. Beijing, China: Science Press, 1998, pp. 148–176.

Libo Yuan, photograph and biography not available at the time of publication.

Wei Jin (M'95–SM'98), photograph and biography not available at the time of publication.

Limin Zhou, photograph and biography not available at the time of publication.

Y. L. Hoo, photograph and biography not available at the time of publication.

M. S. Demokan (SM'89), photograph and biography not available at the time of publication.

Authorized licensed use limited to: IEEE Xplore. Downloaded on October 22, 2008 at 22:21 from IEEE Xplore. Restrictions apply.